Enlargement of step-free SiC surfaces by homoepitaxial web growth of thin SiC cantilevers

Philip G. Neudeck,[a] J. Anthony Powell, Glenn M. Beheim, Emye L. Benavage, and Phillip B. Abel
NASA Glenn Research Center, 21000 Brookpark Road, M.S. 77-1, Cleveland, Ohio 44135

Andrew J. Trunek and David J. Spry
OAI, 21000 Brookpark Road, M.S. 77-1, Cleveland, Ohio 44135

Michael Dudley and William M. Vetter
Department of Materials Science and Engineering, State University of New York at Stony Brook, Stony Brook, New York 11794

Lateral homoepitaxial growth of thin cantilevers emanating from mesa patterns that were reactive ion etched into on-axis commercial SiC substrates prior to growth is reported. The thin cantilevers form after pure stepflow growth removes almost all atomic steps from the top surface of a mesa, after which additional adatoms collected by the large step-free surface migrate to the mesa sidewall where they rapidly incorporate into the crystal near the top of the mesa sidewall. The lateral propagation of the step-free cantilevered surface is significantly affected by pregrowth mesa shape and orientation, with the highest lateral expansion rates observed at the inside concave corners of V-shaped pregrowth mesas with arms lengthwise oriented along the $\langle 1\bar{1}00 \rangle$ direction. Complete spanning of the interiors of V's and other mesa shapes with concave corners by webbed cantilevers was accomplished. Optical microscopy, synchrotron white beam x-ray topography and atomic force microscopy analysis of webbed regions formed over a micropipe and closed-core screw dislocations show that c-axis propagation of these defects is terminated by the webbing. Despite the nonoptimized process employed in this initial study, webbed surfaces as large as 1.4×10^{-3} cm^2, more than four times the pregrowth mesa area, were grown. However, the largest webbed surfaces were not completely free of bilayer steps, due to unintentional growth of 3C-SiC that occurred in the nonoptimized process. Further process optimization should enable larger step-free webs to be realized. © *2002 American Institute of Physics.* [DOI: 10.1063/1.1497456]

I. INTRODUCTION

Substantial progress is being made towards realizing increasingly useful wide band gap SiC and GaN semiconductor electronic devices.[1,2] However, the manufacturing yield, electrical performance, and reliability of these electronic devices is adversely affected by the presence of dislocation defects and nonideal surfaces that arise from the methods presently used to grow and prepare wide band gap crystals for device fabrication. Because large crystals of group III-nitride (III–N) semiconductors (such as GaN) used for device fabrication are generally grown by heteroepitaxy, they contain a high density of dislocations that thread from the substrate/epilayer interface and, in the case of lateral epitaxial overgrowth films, regions of coalescence. In the case of III–N growth on hexagonal SiC substrates, recent studies have shown that many dislocations propagating from the substrate/epilayer interface originate at atomic-scale steps that are left behind on the substrate surface prior to epitaxial growth, despite the use of improved polishing techniques that attain surface to (0001) basal plane tilt angles of about a tenth of a degree.[3] These step-related defects have been

shown to arise even when III–N growth is carried out on well-ordered 6H-SiC terraces with unit (1.5) nm step heights defined by *in situ* pregrowth etching.[4,5] Thus, these works allude to step-free SiC surfaces as being highly beneficial for realizing improved heteroepitaxial III–N films.

Recent studies have experimentally demonstrated that step-free 4H- or 6H-SiC surfaces can be employed to greatly improve the quality of lattice mismatched heteroepitaxial films. In particular, 2-μm-thick (i.e., much greater than the calculated critical thickness for strain relief via dislocation generation) heteroepitaxial films of 3C-SiC (in-plane lattice mismatched to 4H-SiC of $\Delta a/a \sim 0.08\%$) completely free of stacking fault and double-positioning boundary defects were reproducibly grown on step-free 4H-SiC mesa surfaces as large as 0.4 mm×0.4 mm.[6]

Presently, SiC devices are implemented in homoepitaxial films grown on large (presently up to 75 mm in diameter) SiC wafers with surfaces 3°–8° off the (0001) basal plane cut from sublimation-grown boules. In these films, the screw dislocations (both hollow core micropipes and closed-core screw dislocations) that occur in all commercial wafers thread up the crystallographic c-axis to penetrate the entire thickness of the homoepilayer. The occurrence of these defects has been shown to degrade the operation of various SiC

a)Electronic mail: neudeck@grc.nasa.gov

devices.[7–9] The presence of bilayer (or larger) steps on SiC homoepilayer surfaces makes them rough compared to silicon, where it is well documented that oxide–semiconductor interface roughness harms the performance and/or reliability of Si/SiO_2 metal–oxide–semiconductor field effect transistors (MOSFETs).[10,11] Therefore, it is possible that the poor electrical performance and reliability that plagues experimental inversion channel SiC/SiO_2 MOSFETs to date might improve somewhat if smoother, screw dislocation-free SiC epilayer surfaces could be realized.

The process for the formation of SiC mesa surfaces completely free of even a single atomic step was recently reported.[12,13] As described by Powell *et al.*,[12] these surfaces are produced on commercially purchased on-axis 4H- or 6H-SiC wafers by first reactive ion etching trench patterns into the wafer surface to form an array of isolated growth mesas. Pure stepflow epitaxial growth, carried out under conditions that suppress undesired two-dimensional (2D) terrace nucleation of 3C-SiC, is then used to grow all initial surface steps on top of the mesa over to the edge of the mesa, leaving behind a top mesa surface that is completely free of atomic steps. The step-free surfaces produced are of sufficient area to contain entire prototype devices. However, as reported by Powell *et al.*,[12] the high density of screw dislocations limited the yield and size of step free mesas attained on commercial SiC substrates. Mesas that initially contain screw dislocation defects cannot be flattened due to the continual spiral of new growth steps that emanate from screw dislocations during epitaxial growth.

This article presents significant advancements in the growth and characterization of step-free mesas on commercial SiC wafers. In particular, thin lateral cantilevers have been observed to form on mesa surfaces after pure stepflow growth removes almost all atomic steps from the top surface, as initially reported by Neudeck *et al.*[14,15] This article extensively details the observed growth behavior, demonstrating that the lateral propagation of the step-free cantilevered surface is significantly affected by pregrowth mesa shape and crystallographic orientation. Building upon these observations, a SiC homoepitaxial lateral overgrowth process that terminates the *c*-axis propagation of screw dislocations is implemented, thereby enabling larger-area atomically flat surfaces to be realized on commercial SiC wafers.

II. EXPERIMENT

All experiments were carried out on standard commercial ''on-axis'' 4H- and 6H-SiC wafers which had the Si-face side of the wafer polished to within 0.2° of the (0001) basal plane.[16] Mesa patterning (by reactive ion etching trenches) and subsequent epitaxial growth were carried out using the same cold-wall horizontal chemical vapor deposition (CVD) system and general procedures described by Powell *et al.*[12] Table I gives the pregrowth trench depths and epitaxial growth times employed for the five 4H-SiC wafers from which experimental results are presented in this article. As more fully described by Powell *et al.*,[12] the growth process consisted of (1) an *in situ* H_2 etch for 5 min at 1600–1650 °C at a pressure of 100–200 mbar followed by (2) growth at

TABLE I. Experimental wafer process parameters.

Sample No.	Trench depth (μm)	Growth time (h)
1	5–6	0.5
2	12–15	1.0
3	8–10	1.0
4	15–20	1.0
5	15–20	6.0

1600–1650 °C at a pressure of 200 mbar. The sources of Si and C were SiH_4 (2.7 cm^3/min) and C_3H_8 (0.3 cm^3/min), respectively, in H_2 (total flow 4400 cm^3/min). For 4H-SiC homoepilayers grown on 8° off-axis wafers in these reactor conditions, growth rates around 2 μm/h were obtained over the central majority of 2 in. diameter substrates. However, in regions within 5 mm of a wafer edge, the homoepilayer growth rate was observed to rapidly increase with decreasing distance from the wafer edge, to roughly double the growth rate obtained in the wafer central region.

Following epitaxial growth, wafers were characterized initially by Nomarski optical microscopy (NOM) and atomic force microscopy (AFM). AFM scans were taken using either a Digital Instruments Dimension 3000 (DI3000) AFM in tapping mode or a Park Scientific Auto Probe LS AFM in contact mode. The ability of both AFM instruments to clearly reveal 0.5 nm steps was verified on each sample prior to and following measurement of step-free mesas by measuring hillock steps produced on nearby nonflat mesas containing elementary screw dislocations.[12] Following the conclusion of AFM studies, some portions of some samples were studied by scanning electron microscopy (SEM). The reason for completing AFM measurements before conducting SEM was that in previous experiments we noted that our SEM instrument degraded the AFM-revealed surface quality of similar samples. Synchrotron white beam x-ray topography (SWBXT), carried out at beamline X-19C at the National Synchrotron Light Source at Brookhaven National Laboratory, was also used to spatially confirm the presence of screw dislocations at various locations on some samples. Details on SiC dislocation mapping using SWBXT are given by Dudley,[17] but it should be noted that the wafer backside was polished prior to SWBXT in an effort to maximize topographic image clarity by minimizing backside surface roughness.

Regions where unintentional heteroepitaxial growth of 3C-SiC occurred were mapped by thermal oxidation (polytype color mapping and defect delineation following 5 h 1150 °C dry oxidation)[18] and SWBXT as described by Dudley *et al.*[19,20] An important finding of the work of the Dudley *et al.*[19,20] study, which was carried out on a near-edge-region of sample 1 where an abundance of 3C-SiC was unintentionally grown (confirmed by x-ray analysis, oxide color, and the presence of stacking fault features in the oxidized sample), was that regions of 3C-SiC nucleation and growth consistently exhibited 0.25 nm (i.e., single Si–C bilayer thickness) step heights. In contrast, step heights observed in regions of 4H-SiC growth were multiples of 0.5 nm, usually 1.0 nm. Thus, for characterizing the results of growth processes em-
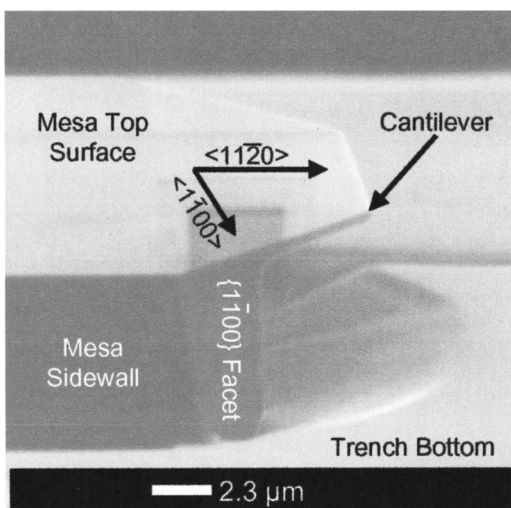
FIG. 1. SEM micrograph of thin lateral 4H-SiC cantilever emanating from mesa top on sample 1 after 30 min of epitaxial growth. The cantilever seamlessly extends the step-free top surface.

ployed in this article, the detection of 0.25 nm growth steps was used as an additional indicator of unintentional 3C-SiC heterogrowth.

III. RESULTS AND DISCUSSION

NOM and AFM studies of 4H-SiC sample 1 of Table I was carried out and reported previously.[12] Elementary screw dislocations were observed to be responsible for the vast majority (>95%) of mesas where steps remained, and resulting growth hillocks were observable by NOM. Nearly identical results were also obtained on the additional samples listed in Table I as well as six other samples (some 6H-SiC) also grown as part of this study. Initial samples (including samples 1–3 in Table I) employed the same pregrowth mesa pattern that predominantly consisted of isolated rectangles and squares ranging in dimension from 50 μm×50 μm to 0.4 mm×0.4 mm. Over a dozen examples of 0.4 mm×0.4 mm step-free surfaces were measured on a wafer (not listed in Table I) with low substrate screw dislocation density.

Closer examination of these initial samples revealed a most interesting growth behavior along the mesa edges. This behavior is summarized below in Figs. 1–2. Figure 1 shows a postgrowth SEM of a mesa sidewall (one of the walls of a square-shaped mesa) on sample 1. A thin lateral cantilever on the order of a micrometer thick is observed emanating from the top of the mesa sidewall, extending outward in the $\langle 11\bar{2}0 \rangle$ direction. The cantilever appears to seamlessly extend the basal plane mesa surface. The thickness of the cantilever appears slightly nonuniform due to thickness variation along the underside. It should be noted that there is no cantilever overhanging the corner region of the square (pregrowth) mesa shape, which appears to have evolved into a small $\{1\bar{1}00\}$ growth facet. Both 4H-SiC and 6H-SiC samples exhibited this behavior.

Figure 2(a) shows an optical micrograph of three 50 μm×50 μm square mesas prior to epitaxial growth, along with a plus-shaped mask alignment mark and letter-shaped mesas which form the acronym "NASA." Figure 2(b) shows
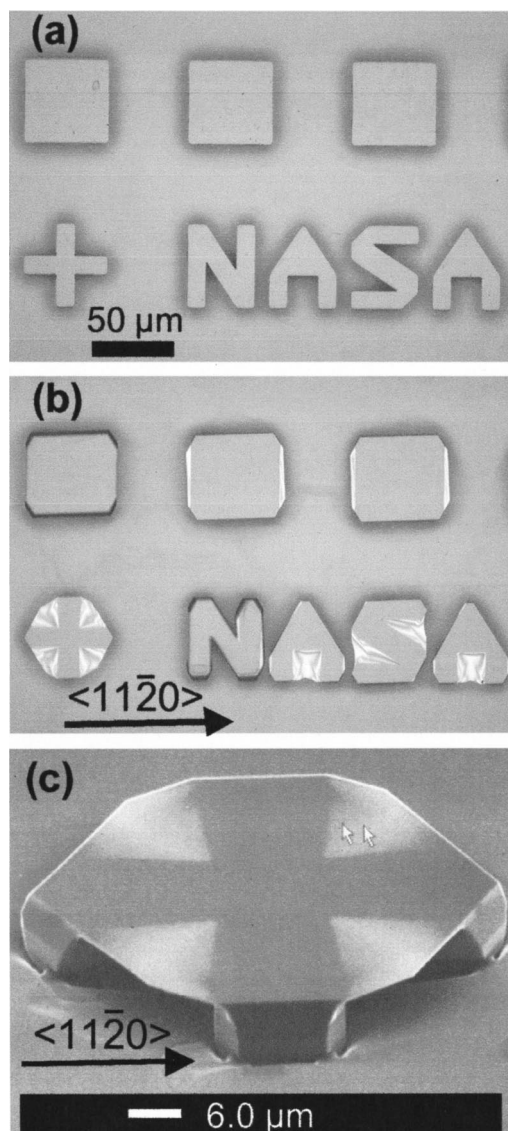

FIG. 2. (a) Optical micrograph of three 50 μm×50 μm mesas, plus-shaped mesa, and letter-shaped mesas prior to epitaxial growth. (b) Optical micrograph of mesa patterns on sample 4 following 1 h of epitaxial growth. Interference fringes are clearly visible where thin cantilevers have formed. (c) SEM micrograph of plus-shaped (pregrowth) mesa on sample 2 following 1 h of epitaxial growth.

the optical appearance of one of these mesa patterns on sample 2 following 1 h of epitaxial growth. The leftmost square mesa and the "N" mesa illustrate the typical optical appearance of postgrowth mesas that contain one or more closed-core screw dislocations prior to epitaxial growth. These mesas grew vertically due to the continual spiral of new growth steps that emanate from the screw dislocations. Thus, the top surface of these mesas with screw dislocations is 2–3 μm higher than the remaining mesas that did not contain screw dislocations.

The remaining mesas in Fig. 2(b) illustrate the typical optical postgrowth appearance of screw dislocation free mesas that have been rendered step-free by the epitaxial growth process. The lighter regions (such as between the arms of the plus-shape) in screw dislocation-free mesas are areas where thin cantilevers have evolved from the top of the mesa side-
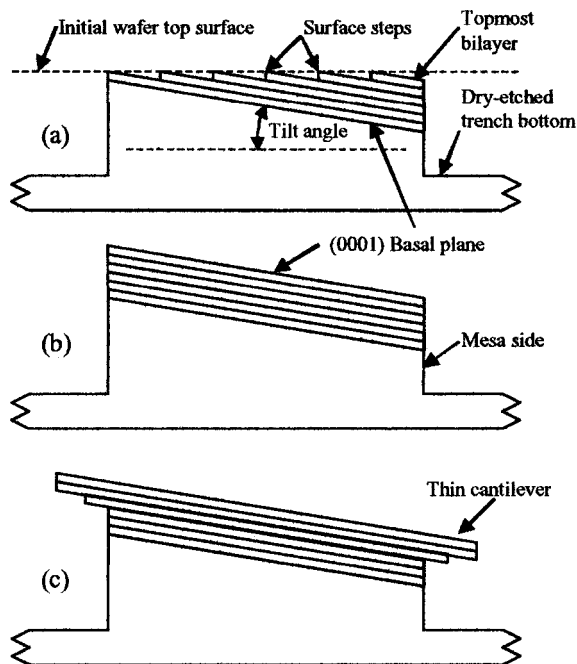
FIG. 3. Simplistic schematic cross-sectional depiction of cantilever formation process. (a) Initial mesa with bilayer steps that arise due to unintentional tilt angle of polished substrate with respect to (0001) basal plane. (b) Step-free mesa formation by carrying out epitaxial growth in pure stepflow conditions with no 2D terrace nucleation and no dislocations to provide growth steps within the mesa. (c) By continuing epitaxial growth, cantilevers are formed as growth adatoms, harvested by the large step-free surface, migrate to the mesa edge where the high bond density leads to incorporation into the crystal near the top of the mesa sidewall. For clarity, the growth that occurs on the lower portions of the vertical mesa sidewalls and the trench bottoms is not depicted.

wall. Optical interference fringes that are particularly visible in the cantilever regions of the plus shape and letters "ASA" are attributed to the interaction of the microscope light with the slight variations in cantilever thickness. Figure 2(c) shows a SEM micrograph of a plus-shaped mesa on sample 3. The epitaxially grown thin lateral cantilevers have completely spanned (or "webbed") the arms of the plus-shaped mesa, forming a seamless nearly hexagonal-shaped "table-top" sitting on top of a cross-shaped support structure. The formation of this structure indicates that enhanced lateral web growth occurred at the inside (i.e., concave) corners of mesa shapes, which combined with hexagonal growth faceting to produce the result shown in Fig. 2. We have descriptively named such features "webbed cantilevers." In addition to web growth, Fig. 2 shows that some sidewall growth also occurred to somewhat expand the plus-shaped support structure.

To explain the formation of the thin lateral cantilevers, we propose the following model depicted by the simplified schematic cross sections of Fig. 3. The initial mesa with steps on the surface is shown in Fig. 3(a). Using the process of Powell *et al.*,[12] pure stepflow growth is then used to grow all steps out of existence as depicted in Fig. 3(b). In the absence of steps, sources of additional steps (e.g., screw dislocation defects), and 2D nucleation on the top of a large step-free surface, vertical epilayer growth in the *c*-axis direction ceases. Nevertheless, growth reactants in the CVD sys-

tem impinge on the large top surface areas and become mobile adatoms that move about on the step-free surface. These mobile adatoms eventually migrate to the mesa edge and onto the mesa sidewall. The favorable bonding (i.e., high bond density) of the mesa sidewall promotes rapid incorporation of adatoms into the crystal before they migrate more than a few micrometers below the top edge of the mesa sidewall, forming thin cantilevers as schematically depicted in Fig. 3(c). As long as conditions are properly maintained to effectively suppress 2D terrace nucleation, the pure stepflow nature of the growth ensures that the top surfaces of the cantilevers are seamless step-free extensions of the basal plane mesa surface. However as depicted in Fig. 3(c), the underside of the cantilever will not grow with a uniform thickness, because the sidewall underneath will grow according to the availability of growth reactants. For clarity, Fig. 3 does not depict growth that occurs on the lower portions of the vertical mesa sidewalls and the trench bottoms.

Cantilevers are not generally observed on simple mesa shapes that contain screw dislocations prior to epitaxial growth. We hypothesize that this is because growth adatoms arriving on such a mesa rapidly incorporate into steps emanating from the screw dislocation hillock, and are therefore not able to migrate to the mesa edge to promote formation of cantilevers. Thus, as discussed by Powell *et al.*,[12] mesas with screw dislocations will experience vertical growth of the mesa top surface instead of the realization of a step-free top surface.

The results of Figs. 1 and 2 clearly indicate that there is a strong directional and shape dependence to cantilever formation consistent with the faceting behavior of hexagonal SiC platelets.[21] For example, on the two mesas towards the right side of Fig. 2(b) (i.e., square mesas without screw dislocations), cantilevers are formed only on the left and right edges where lateral growth extends toward the $\langle 11\bar{2}0 \rangle$ directions. For the case of the nearby plus-shaped mesa [as well as the mesa shown in Fig. 2(c)], the lateral web growth was greatly enhanced at each concave corner of the structure. However, there is no cantilever overhanging the left and right ends of the plus-shaped support structure (i.e., directly toward $\langle 11\bar{2}0 \rangle$) in Fig. 2, as these two ends of the support structure enlarged to $\{1\bar{1}00\}$ facets during the growth. All postgrowth mesas, even those with screw dislocations, exhibited some degree of lateral sidewall expansion and evolution of $\{1\bar{1}00\}$ hexagonal growth facets.

In order to better study the growth of webbed cantilevers, a mask featuring a variety of mesa shapes with inside corners was designed. Pregrowth mesa shapes resembling V's, U's, plus-signs, six-pointed stars (similar to an asterisk character), as well as more complex shapes of various sizes and aspect ratios were etched into on-axis 4H-SiC wafers to a height (i.e., trench depth) between 15 and 20 μm. The epitaxial growth process described earlier was carried out with the growth time increased to 6 h to facilitate more complete webbing of larger structures (sample 5 of Table I). On mesas without screw dislocations, this succeeded in producing thin cantilevers with much greater lateral extension from mesa sidewalls. To study the early evolution of webbing with

J. Appl. Phys., Vol. 92, No. 5, 1 September 2002

Neudeck *et al.* 2395

the mesa shapes, a separate growth run of 1 h was also conducted on a different substrate with the same mesa pattern (sample 4 of Table I).

Figure 4(a) is an optical micrograph of two test mesa V shapes etched into a substrate prior to epitaxial growth. Figure 4(b) shows a sample of the mesa and partial webbing following one hour of growth in the higher growth-rate near-edge region of the substrate. Figures 4(c)–4(e) show three different optical microscopic views of two particular test mesas [that started from the shape depicted in Fig. 4(a)] on sample 5 following the 6 h epitaxial growth. Figure 4(c) shows the postgrowth optical appearance of the two mesas looking from the wafer topside. For mesas that did not initially contain screw dislocations, the 6 h growth time was sufficient to enable complete spanning (i.e., webbing) of the interior portions of the mesas by thin cantilevers. A nearby mesa of the same shape (not shown) did not exhibit appreciable lateral webbing, but instead grew vertically over 15 μm taller than the mesas of Figs. 4(c)–4(e) due to the fact that it initially contained a screw dislocation that provided steps for vertical growth. Strong optical interference fringes were visible in almost all webbed regions, including the webs shown in Figs. 4(b) and 4(c). Consistent with previous figures, these fringes indicate that the webbed regions are thin, but not uniform in thickness due to material growth on the underside of the webbing.

Some noteworthy features are visible in the trench regions of Fig. 4(c). A micropipe (labeled μpipe No. 1) is denoted in the trench region of Fig. 4(c). Additional features denoted are borders between regions of 3C-SiC growth and regions of 4H-SiC growth that occurred in the trenches. The presence of 3C-SiC in trenches was initially indicated by the yellow optical color of the crystal (for sample 5) and double-positioning boundary defects, and confirmed by polytype and stacking fault defect mapping via thermal oxidation.[18,20] This work made no effort to control nucleation and growth in the trenches between mesas for any of the samples. Significant 2D nucleation and growth of 3C-SiC occurred on the trench bottoms of all samples, mixed in with homoepitaxial growth of 4H-SiC. That micropipes are surrounded by 4H-SiC is consistent with the fact that they are screw dislocations which are sources of abundant steps to support SiC homoepitaxy, in agreement with previous studies.[20] The nucleation of 3C-SiC was likely aided by residual plasma etch damage in the trench bottoms. Otherwise, the relative abundance of 3C-SiC in trench bottoms with steps would be inconsistent with the relative absence of 3C-SiC on large step-free mesa surfaces.

Figures 4(d) and 4(e) show two micrographs of the Fig. 4(c) mesas taken looking from the wafer backside. Figure 4(d) was taken looking completely through the transparent SiC wafer to focus on the trench topside surface, while Fig. 4(e) was taken with optical focus on the polished wafer backside surface. Most of the texture observed where the webbing is present in Fig. 4(d) is due to nonuniform material deposition on the trench bottom beneath the webbing. This conclusion is based upon direct topside observation of trench growth beneath webbing on other mesas (not shown) where the webbing was unintentionally shattered by tweezer handling. Similar nonuniform trench deposition is also evident beneath the cantilever shown in Fig. 1. The backside views of the wafer clearly show the presence of a second micropipe, denoted as μpipe No. 2, that can be observed all the
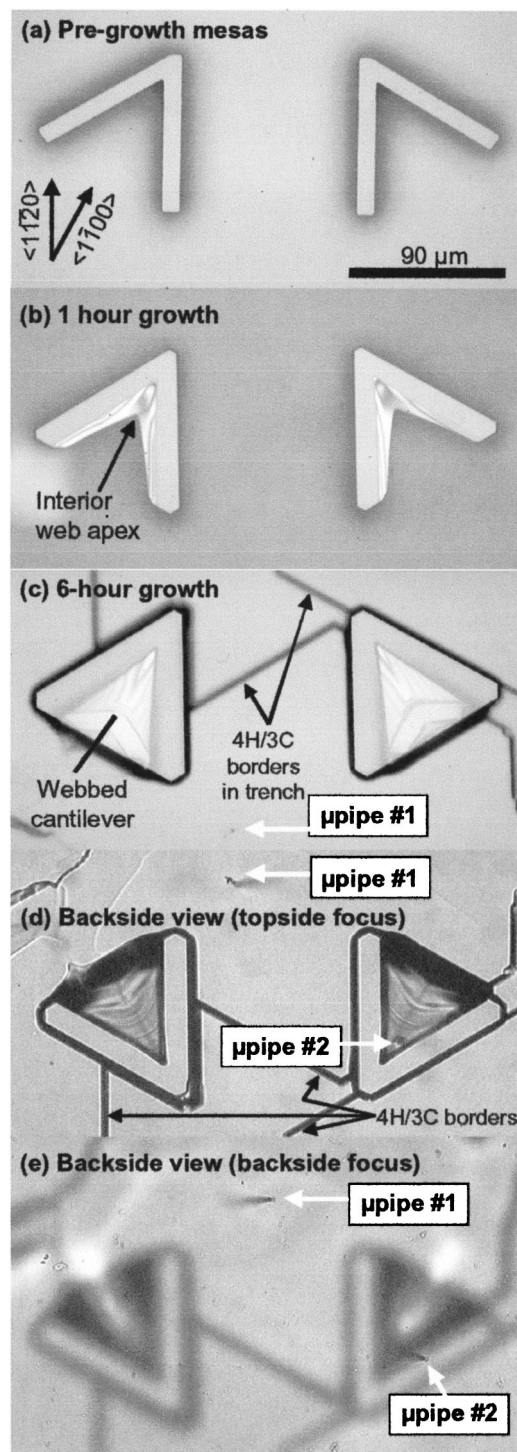

FIG. 4. (a) Optical micrograph of two V-shaped test mesa patterns prior to epitaxial growth. (b) Optical micrograph of thin webbing formed along interior of V shape on sample 4 following 1 h of epitaxial growth. (c) Optical micrograph of thin webbing completely spanning the interior of the V-shaped mesas on sample 5 following 6 h of epitaxial growth. (d) Optical micrograph of same mesas in (c) viewed through the polished wafer backside with the wafer topside in focus. A micropipe (μpipe No. 2) resides beneath the webbing. (e) Same as (d) except the focus is on the wafer backside.

way through the wafer by varying the focus. Figure 4(c) shows that this micropipe intersects the topside trench surface directly beneath the webbing of the right mesa. The fact that there is no sign of this micropipe in the Fig. 4(c) micrograph of the same webbed mesa viewed from the topside indicates that this defect present in the substrate did not propagate into the overgrown webbing. Figures 4(c)–4(e) right mesa was the only instance where a micropipe was observed to reside directly beneath a webbed cantilever, as the rest of the wafer exhibited a much lower micropipe density than the region depicted in Figs. 4(c)–4(e).

In order to confirm the complete absence of the micropipe/screw dislocation from the webbing, the right mesa in Figs. 4(c)–4(e) was studied extensively by AFM, along with a dozen other webbed mesas on the sample. The presence of tall mesas that grew vertically due to screw dislocations on this sample often obstructed the AFM tip from reaching and scanning webbed surfaces of interest. The AFM characterization of webbed regions was made even more difficult due to sinusoidal optical interference measurement artifacts generated by the interaction of the AFM laser with the thin SiC webbing. These artifacts are evident in both scans of Fig. 5, which show AFM scan data from two different AFM instruments of the webbed surface directly over μpipe No. 2 of Figs. 4(c)–4(e). Figure 5(a) was measured with a Digital Instruments Dimension 3000 (DI3000) AFM in tapping mode, while Fig. 5(b) shows the same region measured with a Park Scientific Auto Probe LS AFM in contact mode. The insets of the Fig. 5 scans show AFM cross-sectional line plots that are distinctly different from each other in their periodicity and amplitude. The inconsistency between the two Fig. 5 measurements indicates that the sinusoidal undulations are measurement artifacts. Similar AFM measurement artifacts have been previously observed.[12,22] Despite the presence of optical interference undulations, the DI3000 AFM was nevertheless able to resolve 0.25 nm (i.e., single Si–C bilayer) steps on the surfaces of other webbed regions, as will be discussed later in this article. No steps were observed in a series of scans taken which covered almost the entire top of the right mesa shown in Figs. 4(c)–4(e). Hillocks and steps are always observed on mesas when screw dislocations are present.[12,20] Hence, the absence of hillocks and steps from the mesa/web indicates successful overgrowth of the micropipe screw dislocation defect.

Figures 4(b) and 4(c) illustrate the process of the merging of cantilevers growing on each arm of the V-shaped mesas. AFM scans of the Fig. 4(c) right mesa indicate that the resulting webbed cantilever is step-free, indicating that defect-free merging occurred. Optical and SEM inspection revealed that greater than 95% of cantilevers that merged in a similar manner (i.e., from opposite arms of the same step-free V-shaped or U-shaped mesa) came together to form a featureless top surface free of morphological features in the region of coalescence. While four of these featureless webbed mesas (out of a dozen scanned) were also found by AFM to be completely free of steps, unintentional growth of 3C-SiC (discussed later) prevented the other featureless webbed surfaces on the sample from being classified as completely step-free as measured by AFM.
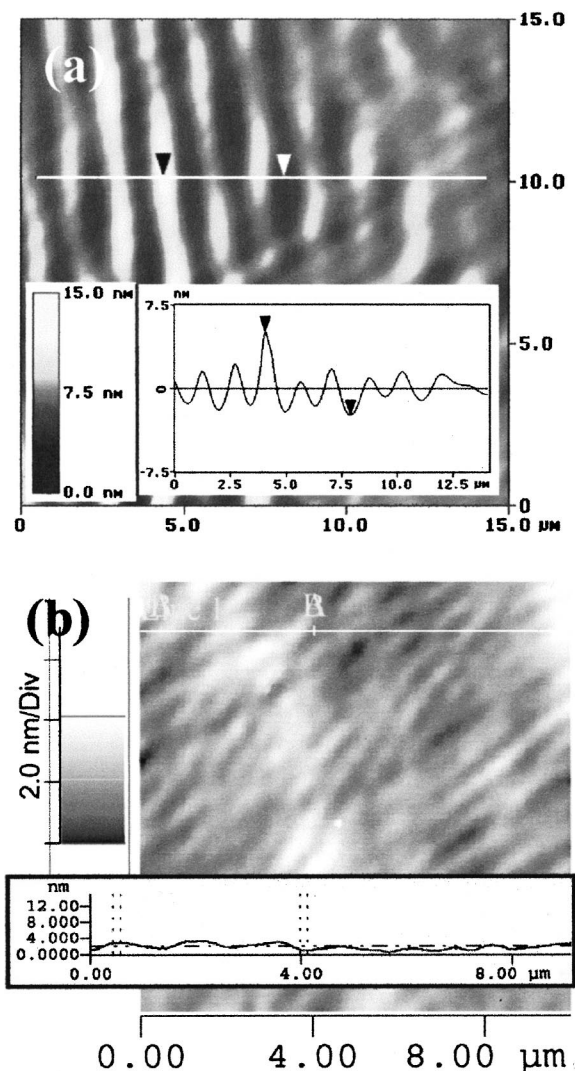

FIG. 5. AFM data of webbed region immediately above Fig. 4(d) μpipe No. 2 measured by (a) DI3000 in tapping mode, and (b) Park Scientific LS in contact mode. Both scans show different undulation characteristics (see cutline plot insets) due to AFM measurement artifacts, but no steps were detected. Additional AFM scans covering the rest of this mesa/webbed surface produced similar profiles, with no steps detected.

In contrast, when thin cantilevers from separated mesa shapes (such as side-by-side rectangles) converged and met during growth, imperfect coalescence was almost always observable by optical microscope or SEM inspection. While the results from nearby mesa pairs were quite variable, it often appeared that the leading edge of one cantilever slipped beneath the leading edge of the opposite approaching cantilever. Detailed experimental study of the exact nature of this imperfect coalescence of separated mesas is beyond the immediate scope and focus of this article. However, by simply placing two figure Fig. 3(c) cross sections next to each other in a side-by-side manner, one can envision how the nonzero tilt angle of the basal plane relative to the original substrate surface may contribute to the observed defective coalescence of cantilevers from separate mesas. We suggest that it would only require a very slight (on the order of 0.25 nm, the height of single Si–C bilayer) vertical deformation at the end of the long (tens of micrometers) thin cantilevers to cause an unfa-

J. Appl. Phys., Vol. 92, No. 5, 1 September 2002
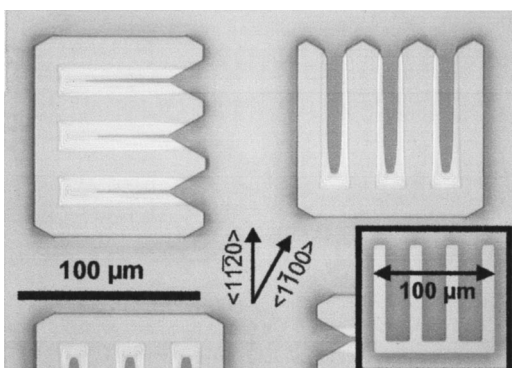
Neudeck *et al.* 2397

FIG. 6. Optical micrograph of webbing on two comb-shaped mesas on sample 4 following 1 h of epitaxial growth. The inset of the figure shows the pregrowth mesa shape. The webbing is more complete for the comb mesa on the left, reflecting the benefits of orienting narrow fingers lengthwise along the $\langle 1\bar{1}00\rangle$ direction.
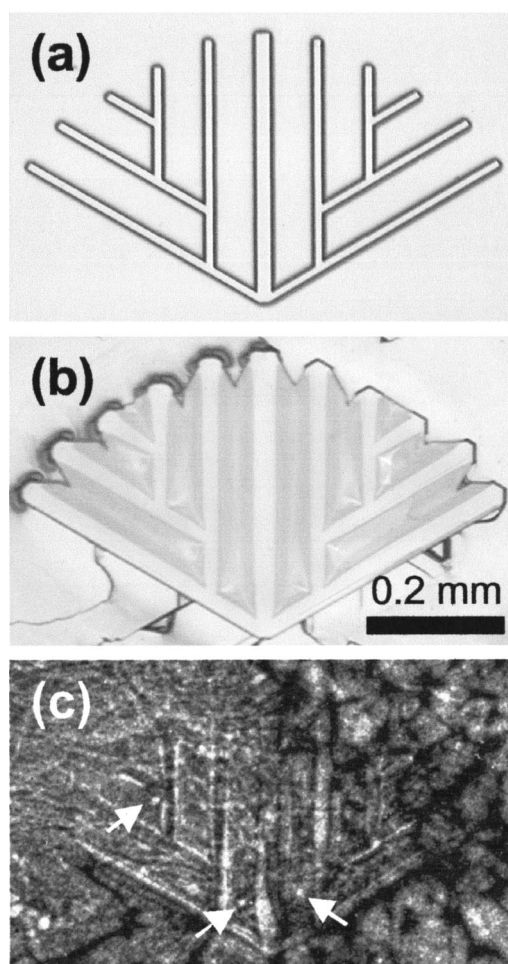

FIG. 7. (a) Optical micrograph of largest pregrowth mesa shape tested in this study. The shape contains joined variations of both U-shaped and V-shaped primitives. (b) Optical micrograph of fully webbed mesa on sample 5 after 6 h of epitaxial growth. (c) Back reflection x-ray topograph of mesa shown in (b). Arrows denote examples of substrate screw dislocations that were overgrown and imaged by x-ray beam penetration through the thin webbing. No evidence of screw dislocation hillocks or 4H-SiC growth steps in the webbing was detected by AFM. However, this surface was not step-free (some 0.25 nm high steps were detected) due to unintentional growth of 3C-SiC.

vorable misalignment of converging cantilevers. We further speculate that such a deformation might be expected to occur during growth due to some combination of thermal gradient effects and/or substrate stress effects. Such small deformations (less than one millionth the length of a cantilever) would probably result in misalignment of the stacking sequence when one cantilever laterally meets up with the opposite cantilever.

Our experimental results indicate that open mesa shapes with continuous top step-free surfaces facilitate highly ordered joining of cantilevers evolving from opposite arms of the shape to occur. In particular, the V-shape mesa [such as Fig. 4(a)], after it has been rendered entirely step-free during the initial stages of growth, appears to enable an ordered "zippering" together of cantilevers growing from opposite arms of the structure. As is evident in Fig. 4(b), the joining of the two cantilevers occurs in a progressive fashion along an outwardly moving apex [denoted as "interior web apex" in Fig. 4(b)] where the interior cantilevers from the two sides of the V intersect. As the web expands, the top bilayers of the web apex act as a site where growth adatoms spilling off the step-free surface preferentially incorporate. Both sides of the apex have the same (step-free) basal plane top surface, and the high bond density on the leading edge sidewall of the cantilever ensures adatom incorporation into the crystal very near to the topmost bilayer. Therefore, we propose that the joining of cantilevers occurs in vertical registration as the interior web apex is grown outward, enabling the observed step-free top surface throughout the region of joining.

The U-shaped mesa primitive also exhibited well-ordered joining of cantilevers in a similar manner as the V-shape mesa primitive. Figure 6 shows the evolution of two differently oriented "comb" shaped mesas following 1 h of growth. The pregrowth shape, illustrated in the Fig. 6 inset, is a conjunction of three U-shaped mesa primitives (with right-angle interior corners). Following growth, the long fingers of the left comb are noticeably more webbed than the fingers of the right comb, consistent with the preference of cantilevers to grow toward the $\langle 11\bar{2}0\rangle$ direction to form $\{1\bar{1}00\}$ facets. On the left comb, convergence of cantilevers expanding vertically from the horizontal fingers has taken

place on the left third of the structure. The enhanced growth in the interior of each U enables well-ordered coalescence from the separate arms (i.e., fingers) to proceed along an outwardly moving coalescence apex in a similar manner as the V shape. For both postgrowth mesas of Fig. 6, there is negligible cantilevering observed on the shape exterior (i.e., the three nonfingered sides). However, the mesa support structure laterally enlarged to form $\{1\bar{1}00\}$ facets on the exterior sides.

Larger web growth test mesas were constructed from joined multiple combinations of V- and/or U-shaped mesa primitives. Figure 7 illustrates experimental results from such a structure, which is the largest tested in our experiments to date. The Fig. 7(a) optical micrograph illustrates the mesa shape prior to growth, while the Fig. 7(b) optical micrograph shows a fully webbed structure on sample 5 following the 6 h growth. The size of the fully webbed surface
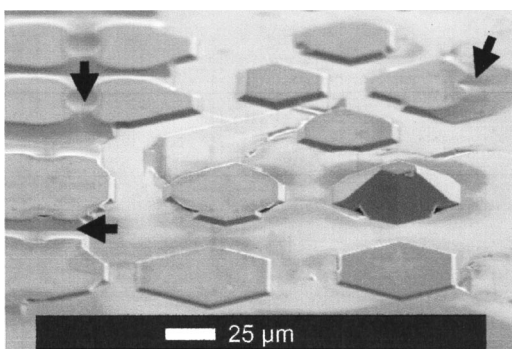
FIG. 8. SEM micrograph taken on sample 5 following 6 h of epitaxial growth. Arrows denote examples of where uncontrolled trench growth has clearly merged with the top surface of a mesa/webbing. A screw dislocation enabled vertical growth of the tallest mesa shown in the SEM image. The hexagon-shaped surface immediately above the distance scale evolved from an asterisk-shaped pregrowth mesa faintly visible in the SEM image.

$(>1.4 \times 10^{-3} \text{ cm}^2)$ is more than four times the top surface area of the pregrowth mesa.

Figure 7(c) shows a postgrowth backreflection x-ray topograph of the same mesa. In backreflection x-ray topographs, *c*-axis screw dislocations appear as white circles surrounded by black rings of various diameters.[23] While AFM and NOM inspection of some of these webbed regions revealed no screw dislocation hillocks, spirals, or associated 0.5 or 1.0 nm high steps, images of closed-core *c*-axis screw dislocations could be noted in the x-ray topographs. In Fig. 7(c), for example, three screw dislocation images (denoted by arrows) reside between the fingers of the mesa where there is webbing. The characteristic *c*-axis screw dislocation image in these cases is somewhat obscured, apparently because the screw dislocations are confined to the substrate (within the trenches, as was the micropipe of Fig. 4) and were therefore imaged with penetration of the incident and diffracted x-ray beams through the thin webbing.

It should be noted that for larger and more complex pregrowth mesa shapes [such as the shape of Fig. 7(a)], some limited regions exhibited cantilever formation despite the presence of a screw dislocation hillock in the pregrowth mesa. In these cases, the cantilevering occurred in fingered regions away from the finger with the screw dislocation, and/or to a much lesser lateral extent than nearby fingered mesas without screw dislocations.

Figure 8 shows a SEM micrograph of part of the sample 5 wafer surface where all but one of the pregrowth mesas was free of screw dislocations and experienced complete webbing. For example, the mesas directly above the SEM scale mark webbed into hexagons starting from asterisk pregrowth mesa shapes. It can be seen in Fig. 8 that material grown in the trenches rose nearly to the level of the mesa/webbing top surface in this region of the wafer. This occurred because vertical growth on the top of defect-free mesas ceases, while screw dislocations and uncontrolled 3C-SiC nucleation caused vertical growth in the trenches. The arrows in Fig. 8 indicate some of the places where trench growth clearly merged with the top of the mesa/webbing. In cases where trench growth merged with mesa/webbing tops, AFM measured 0.25 nm steps consistent with stepheights

observed for 3C-SiC (inconsistent with 0.5 and 1.0 nm stepheights observed for on-axis epitaxial 4H-SiC).[20] The presence of 3C-SiC on such mesas was further confirmed by subsequent thermal oxidation (polytype and stacking fault defect) mapping of a small piece of the sample 5 wafer.[18] This is consistent with the fact that most regions of trench growth on the sample were shown to be 3C-SiC. In Fig. 7(b), the ends of the mesa fingers near the ''(b)'' demonstrate the optical appearance of a region of trench growth and mesa/webbing merging. This contrasts with the optical appearance of the finger ends on the right half of the Fig. 7(b) mesa, which may not have merged perhaps due to some combination of surface tilt angle and nonuniform trench growth. Thus, it is not surprising that 0.25 nm high steps (indicating 3C-SiC heterogrowth) were observed on the surface of the Fig. 7(b) mesa/webbing. To favorably inhibit trench growth from rising up to interfere with the step-free surface, patterned selective growth masking techniques, such as the graphitic masking technique reported by Eshun *et al.*[24] for SiC, could be employed.

The initial experimental results presented here indicate that the rate of 2D nucleation of 3C-SiC on the 4H-SiC basal plane surface can be made small enough (i.e., close enough to zero) to enable formation of relatively large step-free 4H-SiC surfaces and cantilevers. It is worth noting that the results of this study are inconsistent with the much higher nucleation probabilities reported by Kimoto and Matsunami,[25] but important experimental differences (including pregrowth surface preparation procedure and growth process parameters) are probably responsible for this discrepancy. Despite the near-zero nucleation probabilities demonstrated in the present study, 3C-SiC was nevertheless observed by AFM (0.25 nm steps) and thermal oxidation mapping on some mesas/webs that did not experience merging with trench growth. For growth times of an hour or less, less than 5% of mesas in the central regions of wafers experienced 2D nucleation and growth of 3C-SiC. After 6 h of growth (sample 5), a majority of webbed mesas that appeared free of trench growth merging experienced growth of 3C-SiC. Therefore, the 2D nucleation probability in these growth conditions is not equal to zero.

In light of previous studies that have linked the probability of 3C-SiC nucleation to the average basal plane terrace width (via substrate tilt angle),[26,27] it stands to reason that the probability of 3C-SiC nucleation also increases with step-free surface width. As the webbing enlarges the step-free surface area during growth, the probability of 2D nucleation of 3C-SiC should also increase. Furthermore, the step-free surface should also harvest more mobile adatoms as its collection area enlarges. If the surface adatom mobility is sufficiently high, such that adatoms do not return to the gas flow or 2D nucleate 3C-SiC before migrating to incorporate into the mesa/webbing perimeter, an increased flow of adatoms would be supplied to the step-free surface perimeter to contribute to cantilever growth. Under these assumed circumstances, the cantilever expansion rate might be expected to increase as the area [more accurately, the area-to-perimeter ratio (A/P)] of the step-free surface increases with growth time.

With the earlier discussion in mind, the narrow fingered comb shape, oriented as illustrated on the left side of Fig. 7, exhibits a number of advantages that potentially facilitate rapid expansion of the step-free web. First, it takes advantage of the previously noted faster cantilever growth toward the $\langle 11\bar{2}0 \rangle$ direction for fingers oriented lengthwise in the $\langle 1\bar{1}00 \rangle$ direction. Second, as discussed in the previous paragraph, the narrow rectangular fingers of the comb shape facilitate the most rapid increase in area and A/P to most rapidly increase growth adatom collection and rate of cantilever expansion. Third, as the cantilevers begin to merge, as for example is illustrated in the left third of the left Fig. 7 comb, the perimeter is further reduced which favorably increases A/P which could lead to even more rapid expansion of remaining interior cantilevers. By shrinking the width (but not length) of each comb finger (as well as the base connecting the fingers), the pregrowth mesa area could be shrunk to beneficially reduce the probability of the pregrowth mesa being threaded by a substrate screw dislocation. Such feature shrinkage would of course suffer the partial drawback that somewhat increased epitaxial growth time would be needed to achieve complete webbing. Finally, if one ascertained the direction of unintentional tilt in the substrate, the comb could be oriented with its open end oriented toward the $\langle 1\bar{1}00 \rangle$ direction closest to the pregrowth tilt direction (i.e., the stepflow direction). This orientation would enable the base of the comb to contain the topmost bilayer [Fig. 3(a)], so that initial stepflow needed to establish the step-free surface could proceed from the base of the comb down the fingers.

Further experiments, well beyond the initial data reported in this article, are required to better understand and quantify the time-varying rate of web evolution and 2D nucleation. Likewise, further experiments might also optimize epitaxial growth conditions with the goal of increasing cantilever growth rate while better suppressing 2D nucleation of 3C-SiC. Towards this end, higher temperature CVD epitaxial techniques, such as those reported by Kordina *et al.*[28,29] that have achieved much faster off-axis growth rates than the reactor used in this work, should enable increased growth rate and surface adatom mobility favorable to realizing larger step-free webbed cantilevers. The degree to which these goals can be achieved, coupled with the substrate screw dislocation density, will determine practical limits as to the size of step-free surfaces that can be realized using a more optimized SiC web growth process. Further process optimization experiments are planned, with a near-term goal of achieving a better than 50% step-free yield for webbed surface areas in excess of 1 mm×1 mm on commercial SiC wafers. The realization of larger webs and step-free surface areas could lead to improved wide band gap microelectromechanical and power devices.

IV. SUMMARY

The homoepitaxial growth of thin lateral cantilevers emanating from step-free 4H-SiC mesa surfaces was accomplished. Enhanced cantilever growth was obtained at concave mesa corners, permitting the realization of webbed structures that can significantly enlarge the step-free surface area produced by selected mesa shapes. The lateral webbing overgrows *c*-axis screw dislocations (including micropipes) that are located in trenches between mesa structures. This enables step-free surfaces to be formed on top of these defects. Thus the area limitation that SiC substrate screw dislocations previously imposed on realizing step-free surfaces can be largely overcome with proper selection of pregrowth mesa shape. The realization of larger step-free SiC surfaces could permit improvements in both the performance and size of wide band gap electronic devices realized by heteroepitaxial growth.

[1] P. G. Neudeck, in *The VLSI Handbook*, edited by W. K. Chen (CRC Press and IEEE Press, Boca Raton, FL, 2000), pp. 6.1–6.24.

[2] S. J. Pearton, J. C. Zolper, R. J. Shul, and F. Ren, J. Appl. Phys. **86**, 1 (1999).

[3] S. Tanaka, R. S. Kern, and R. F. Davis, Appl. Phys. Lett. **66**, 37 (1995).

[4] S. Yamada, J. Kato, S. Tanaka, I. Suemune, Y. Aoyagi, N. Teraguchi, and A. Suzuki, presented at Materials Research Society Fall Meeting, Boston, MA, 2000 (unpublished).

[5] S. Yamada, J. Kato, S. Tanaka, I. Suemune, A. Avramescu, Y. Aoyagi, N. Teraguchi, and A. Suzuki, Appl. Phys. Lett. **78**, 3612 (2001).

[6] P. G. Neudeck, J. A. Powell, A. J. Trunek, W. M. Vetter, and M. Dudley, in *Silicon Carbide and Related Materials 2001*, edited by S. Yoshida, S. Nishino, H. Harima, and T. Kimoto (Trans Tech, Switzerland, 2002), pp. 311–314.

[7] P. G. Neudeck and J. A. Powell, IEEE Electron Device Lett. **15**, 63 (1994).

[8] P. G. Neudeck, W. Huang, and M. Dudley, IEEE Trans. Electron Devices **46**, 478 (1999).

[9] Q. Wahab, A. Ellison, A. Henry, E. Janzén, C. Hallin, J. D. Persio, and R. Martinez, Appl. Phys. Lett. **76**, 2725 (2000).

[10] D. K. Schroder, *Advanced MOS Devices*, Modular Series on Solid State Devices 7 (Addison-Wesley, Reading, MA, 1987), pp. 204–208.

[11] S. Takagi, A. Toriumi, M. Iwase, and H. Tango, IEEE Trans. Electron Devices **41**, 2357 (1994).

[12] J. A. Powell, P. G. Neudeck, A. J. Trunek, G. M. Beheim, L. G. Matus, J. R. Hoffman, and L. J. Keys, Appl. Phys. Lett. **77**, 1449 (2000).

[13] J. A. Powell, P. G. Neudeck, A. J. Trunek, G. M. Beheim, L. G. Matus, R. W. Hoffman, Jr., and L. J. Keys, presented at Electronic Materials Conference, Denver, CO, 2000, Late News.

[14] P. G. Neudeck, J. A. Powell, A. Trunek, G. Beheim, and D. Spry, presented at Electronic Materials Conference, Notre Dame, IN, 2001 (The Minerals, Metals & Materials Society), p. 47.

[15] P. G. Neudeck, J. A. Powell, A. Trunek, D. Spry, G. M. Beheim, E. Benavage, P. Abel, W. M. Vetter, and M. Dudley, in *Silicon Carbide and Related Materials 2001*, edited by S. Yoshida, S. Nishino, H. Harima, and T. Kimoto (Trans Tech, Switzerland, 2002), pp. 251–254.

[16] Cree, Inc., 4600 Silicon Drive, Durham, NC 27703.

[17] M. Dudley, in *Encyclopedia of Applied Physics* (Wiley, New York, 1997), Vol. 21, pp. 533–547.

[18] J. A. Powell *et al.*, Appl. Phys. Lett. **59**, 183 (1991).

[19] M. Dudley, W. M. Vetter, X. Huang, P. G. Neudeck, and J. A. Powell, in *Silicon Carbide and Related Materials 2001*, edited by S. Yoshida, S. Nishino, H. Harima, and T. Kimoto (Trans Tech, Switzerland, 2002), pp. 391–394.

[20] M. Dudley, W. M. Vetter, and P. G. Neudeck, J. Cryst. Growth **240**, 22 (2002).

[21] S. G. Muller, R. Eckstein, R. F. P. Grimbergen, D. Hofmann, and B. Rexer, in *Silicon Carbide, III-Nitrides, and Related Materials*, edited by G. Pensl, H. Morkoc, B. Monemar, and E. Janzen (Trans Tech, Switzerland, 1998), pp. 425–428.

[22] *Scanning Probe Microscopy Notebook, Rev. 3.0* (Digital Instruments, Santa Barbara, CA, 1998), p. 52.

[23] M. Dudley, W. Huang, S. Wang, J. A. Powell, P. Neudeck, and C. Fazi, J. Phys. D **28**, A56 (1995).

[24] E. Eshun, C. Taylor, M. G. Spencer, K. Kornegay, I. Ferguson, A. Gurray, and R. Stall, in *Wide-Bandgap Semiconductors for High Power, High Frequency and High Temperature Applications—1999*, edited by S. C.

Binari, A. A. Burk, M. R. Melloch, and C. Nguyen (Materials Research Society, Warrandale, PA, 1999), pp. 173.

[25] T. Kimoto and H. Matsunami, J. Appl. Phys. **78**, 3132 (1995).

[26] H. Matsunami, K. Shibahara, N. Kuroda, W. Yoo, and S. Nishino, in *Amorphous and Crystalline Silicon Carbide*, Springer Proceedings in Physics 34, edited by G. L. Harris and C. Y.-W. Yang (Springer, Berlin, 1989), pp. 34–39.

[27] J. A. Powell *et al.*, Appl. Phys. Lett. **59**, 333 (1991).

[28] O. Kordina *et al.*, Appl. Phys. Lett. **69**, 1456 (1996).

[29] O. Kordina, C. Hallin, A. Henry, J. P. Bergman, I. Ivanov, A. Ellison, N. T. Son, and E. Janzen, Phys. Status Solidi B **202**, 321 (1997).